Available online at www.sciencedirect.com
SCIENCE DIRECT®
Journal of Nuclear Materials 337–339 (2005) 505–509
journal of nuclear materials
www.elsevier.com/locate/jnucmat

Thermal wall load control using fast gas puffing in the TPE-RX reversed-field pinch

H. Sakakita *, Y. Yagi, H. Koguchi, Y. Hirano, T. Shimada

National Institute of Advanced Industrial Science and Technology (AIST), Tsukuba Central 2, 1-1-1 Umezono, Tsukuba, Ibaraki 305-8568, Japan

Abstract

In order to reduce the thermal wall load due to the phase- and wall-locked modes particularly in the high plasma current regime, neutral gas puffing experiments have been conducted in the TPE-RX reversed-field pinch. The temperature of the plasma-facing wall at the mode-locking position sometimes exceeds the melting temperature of stainless steel. It has been determined that the maximum temperature increment of the wall becomes almost half in the neon and deuterium gas puffing cases at a plasma current of 350 kA. This indicates that neutral gas puffing can reduce the severe thermal wall load. The radiative cooling around the peripheral region as a result of neon gas puffing and the decrease in the heat flux along local magnetic field lines as a result of deuterium gas puffing are possible reasons behind the decrease in the rate of energy flow to the wall.

PACS: 52.25.Y; 52.30; 52.40.H; 52.70
Keywords: First wall; Gas injection and fueling; Neon; Power deposition; Radiation

1. Introduction

In a reversed-field pinch (RFP), spatially localized and temporary stationary structures, i.e., the phase- and wall-locked modes, cause severe thermal load enhancement to the wall at the mode-locking position during high plasma current, I_p, operation [1,2]. In the TPE-RX RFP device at the National Institute of AIST, the estimated heat flux is $\sim$100 MW/m^2 at the mode-locking position. The estimated temperature of the inner surface of the vacuum vessel sometimes exceeds the melting temperature of stainless steel [3]. The total input energy and the wall temperature increase as I_p increases. Therefore, in order to conduct experiments in the high I_p regime, it is necessary to mitigate the enhanced thermal wall load due to the locked mode.

As an attempt to mitigate the thermal wall load, a rotating $m = 0$, $n = 1$ magnetic field perturbation using an additional toroidal coil system is applied in TPE-RX. m and n indicate poloidal and toroidal magnetic mode numbers, respectively. As a result, the locked mode can be successfully removed [4]. This technique is effective up to $I_p = 250$ kA, but above that current we need another method to reduce the thermal wall load. In tokamaks, radiative cooling of the edge plasma and divertor via neutral gas puffing has been conducted [5]. In some of these studies, improved confinement

* Corresponding author. Tel.: +81 29 861 5775; fax: +81 29 861 5754.
E-mail address: h.sakakita@aist.go.jp (H. Sakakita).

0022-3115/$ - see front matter © 2004 Elsevier B.V. All rights reserved.
doi:10.1016/j.jnucmat.2004.10.049

occurs with impurity gas seeding [6]. In the RFX RFP, a radiative mantle was established in high electron density discharges with neon gas puffing [7].

In order to study the changes in thermal wall load, we conducted fast gas puffing using neutral gas in TPE-RX. The results are reported here.

2. Experimental setup

TPE-RX (R/a = 1.72/0.45 m, where R and a are the major and minor radii, respectively) has a multilayered shell system that provides magnetohydrodynamic mode stabilization and equilibrium control. The shell proximity is b/a = 1.08 (b is the minor radius of the innermost shell). The vacuum vessel is made of 316 L stainless steel with fixed molybdenum limiters. Global confinement properties under standard operating conditions, at plasma current, I_p < 500 kA, are in the range of poloidal beta, β_p = 5–10%, and the energy confinement time, τ_E = 0.5–1 ms, with a relatively high I_p/N value of 12×10^{-14} A which is almost constant for I_p = 200–400 kA [8]. N is the column density. The standard operating conditions are characterized by feedback-controlled gap-error field compensation and with a prefilled deuterium gas (D_2).

In order to mitigate the thermal wall load during discharges, two fast-acting electromagnetic valves (FAVs) are installed at the bottom ports of the TPE-RX vacuum vessel with a toroidal separation of 180° as illustrated in Fig. 1. The amount of puffed gas is adjusted by changing the absolute back pressure of the FAV, P_{GP}, and keeping the gate pulse width (4.6 ms) and the applied voltage of the puffing valve constant. P_{GP} of 70 kPa and 400 kPa using two valves approximately correspond to 7 Pa m^3/s for neon gas (Ne) and 200 Pa m^3/s for D_2. Gas puffing is always triggered at t = 20 ms which approximately corresponds to the end of the current-rise phase. Chromel-constantan thermocouples (TCs) attached to the vessel outer surface of the bellows valley are used to monitor the wall temperature, T_w [9]. In the present study, a toroidal array of 36 TCs on the outboard side in the equatorial plane is used. The central electron temperature (T_{e0}) and electron density (n_{e0}) are measured using a single-pulse, single-point Thomson scattering system. The line-averaged electron density (n_{el}) is measured using a two-color, heterodyne CO_2 interferometer. D_2 is used as an operating gas, and prefilled to 93 mPa in advance of the discharge.

3. Experimental results

Fig. 2(a)–(c) show shot-averaged time evolutions of I_p, the one-turn loop voltage, V_{loop}, and the reversal parameter, $F = B_{tw}/\langle B_t \rangle$, respectively, in the standard no-gas puffing case, Ne puffing case with P_{GP} = 26 kPa, and D_2 puffing case with P_{GP} = 400 kPa. Here, B_{tw} and $\langle B_t \rangle$ are the toroidal magnetic field on the plasma surface and the volume-averaged toroidal magnetic field, respectively. Note that gas puffing is conducted without

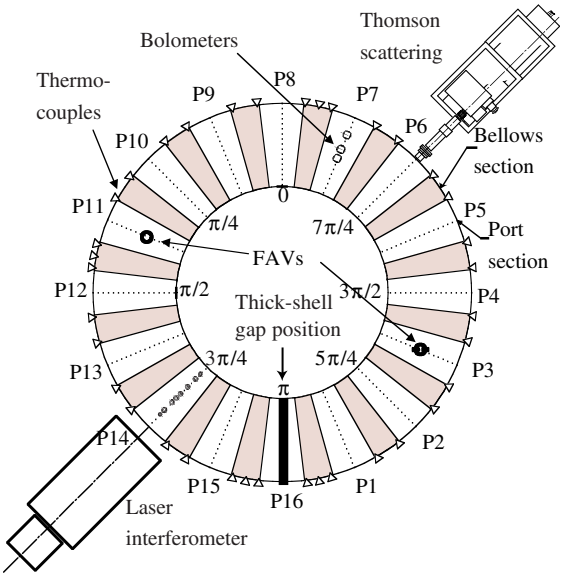

Fig. 1. Schematic drawing showing the locations of the thermocouples, laser interferometer, Thomson scattering and two fast-acting valves.

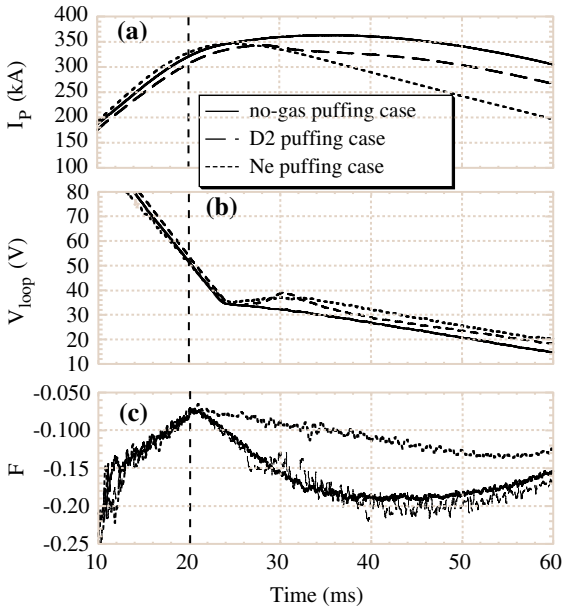

Fig. 2. Shot-averaged waveforms of (a) I_p, (b) V_{loop} and (c) F in the no-gas puffing, Ne puffing and D_2 puffing cases.

changing the charging voltages for the poloidal circuits, so that, particularly after gas puffing at $t = 20$ ms, I_p decays slightly and a slight increase in V_{loop} due to the increase in plasma resistance is observed. F in the D_2 puffing case fluctuates as shown in Fig. 2(c) [10]. Note that F in the Ne puffing case is less negative, since the setting voltage of the reversal capacitor bank is smaller than those of the other two cases.

Fig. 3(a) and (b) show the time evolutions of $n_{el}(r/a)$ at $r/a = 0.0$ and 0.69, respectively, in the no-gas puffing case and Ne puffing case at 26 kPa at $I_p = 300$ kA discharges. Both n_{el} values at $r/a = 0.0$ and 0.69 increase by ~10 ms after gas puffing, reach a maximum at $t = \sim 30$ ms, and then gradually decay. The ratio, $n_{el}(0.69)/n_{el}(0)$, reaches ~0.9 at $t = 31$ ms as shown in Fig. 3(c). If it is assumed that $n_{el}(0.69)/n_{el}(0) = \{1 - (r/a)^2\}^{\alpha}$, then the ratio becomes ~0.9 with $\alpha \sim 0.16$. In the case of a parabolic density profile, the ratio becomes 0.53 with $\alpha = 1$. Therefore, the electron density profile flattens considerably. In the D_2 puffing case, it was confirmed that the electron density profile becomes broader or even hollow as P_{GP} increases [10].

In our previous studies [2,11], it was confirmed that a toroidally localized temperature peak measured by the 36 TC array corresponds approximately to the mode-locking position, which is detected by the top and bottom radial magnetic field sensor arrays. The wall temperature, T_w, is measured by the toroidal array of TCs at 13 s after the end of the discharge (T_w reaches a maximum at 13 s after each discharge). It is observed that T_w increases as I_p increases, and a maximum wall temperature increment, $T_{w\text{-}max}$, reaches 57 degrees centigrade (°C) at $I_p = 350$ kA, which corresponds to ~2300 °C on the plasma-facing side of the vessel. Thus, the continuous locked mode at the same location might cause severe damage to the bellows. Fig. 4(a) and (b) show 4-shot examples of the toroidal distributions of the temperature increment in the Ne puffing case of 26 kPa and the D_2 puffing case of 400 kPa at $I_p = 350$ kA, respectively. As observed in Fig. 4(a) and (b), the peak values at T_w at the mode-locking position vary shot by shot, and $T_{w\text{-}max}$ decreases from 60 °C to 30–40 °C. Fig. 4(c) shows a histogram for the $T_{w\text{-}max}$ distribution of 40 discharges, which include the Ne puffing cases of 9, 25, 26, 30, 40, 49 and 70 kPa. Note that $T_{w\text{-}max}$ varies widely from 5.3 to 42.4 °C, with the highest frequency appearing asymmetrically in the lower part of $T_{w\text{-}max}$ (10–20 °C).

Fig. 5(a) and (b) show dependencies of $T_{w\text{-}max}$ and average wall temperature increment measured by the 36 TCs, $T_{w\text{-}avg}$, on P_{GP} at $I_p = 350$ kA, respectively. (Here, note that 10 Ne puffing shots and 50 D_2 puffing shots are used for each P_{GP} case, respectively.) As shown in Fig. 5(a), in the Ne puffing case, $T_{w\text{-}max}$ begins to decrease with a small amount of Ne puffing, while in the D_2 puffing case, $T_{w\text{-}max}$ decreases at $P_{GP} > 200$ kPa, and $T_{w\text{-}max}$ becomes half at the highest P_{GP} of 200 Pa m^3/s. As shown in Fig. 5(b), $T_{w\text{-}avg}$ decreases in the Ne puffing case, while in the D_2 puffing case, $T_{w\text{-}avg}$ does not decrease significantly with P_{GP}. The decrease in $T_{w\text{-}max}$ corresponds to the mitigation of the plasma–wall interaction enhanced by the locked mode. This result indicates that the neutral gas puffing in the RFP plasma can reduce the severe thermal wall load.

The confinement property, β_p, slightly decreases from 9.0 ± 3.5 (no-gas puffing case) to 8.4 ± 2.0 (Ne puffing

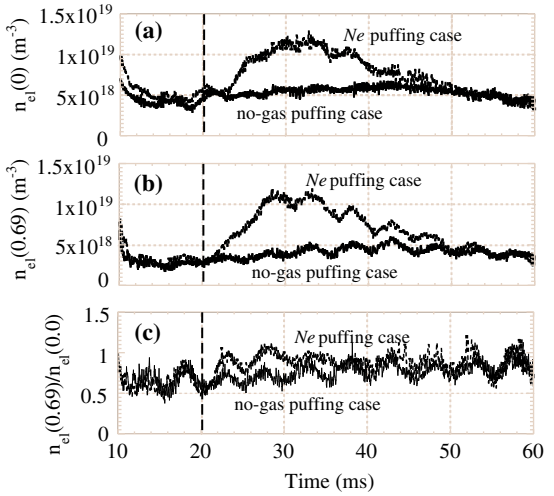

Fig. 3. Line-averaged electron densities, (a) $n_{el}(0)$, (b) $n_{el}(0.69)$ and (c) $n_{el}(0.69)/n_{el}(0)$, for the no-gas puffing and Ne puffing cases.

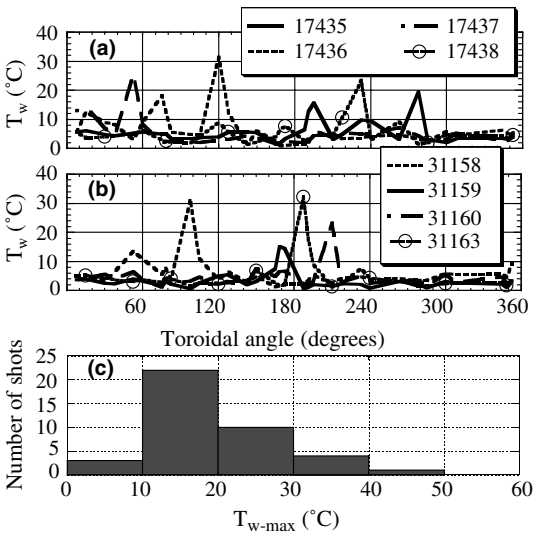

Fig. 4. Typical toroidal distributions of the temperature increment of TCs, (a) Ne puffing and (b) D_2 puffing cases. (c) Histogram of the $T_{w\text{-}max}$ distribution of 40 discharges in the Ne puffing case.

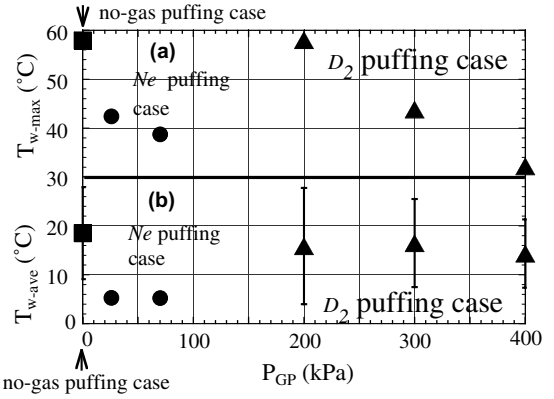

Fig. 5. (a) $T_{w\text{-}max}$ and (b) $T_{w\text{-}avg}$ as functions of P_{GP} in the no-gas puffing case (squares), the Ne puffing cases (circles) of 26 and 70 kPa, and the D_2 puffing cases (triangles) of 200, 300 and 400 kPa at $I_p = 350$ kA. Error bars correspond to standard deviation.

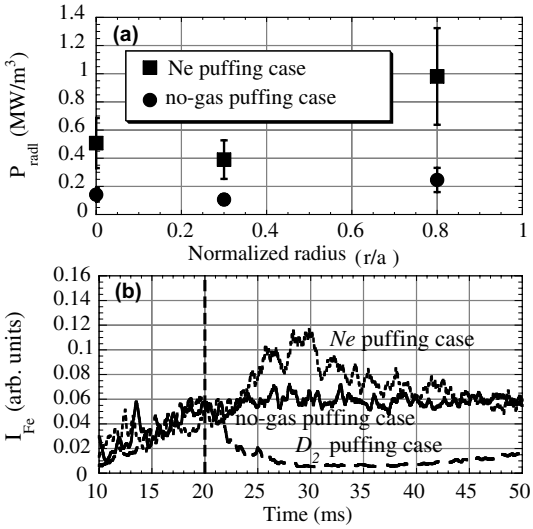

Fig. 6. (a) Line-averaged radiated power per unit volume at $r/a = 0$, 0.31 and 0.8, in the no-gas puffing and Ne puffing cases (35% of each value approximates the error bar [12]) and (b) smoothed waveforms of iron neutral line emission of 390.1 nm in the no-gas puffing, Ne puffing and D_2 puffing cases.

case) at $I_p = 300$ kA; however, τ_E decreased due to the increase in the ohmic input power, P_{oh}. Here, parabolic and flat pressure profiles are assumed in the no-gas puffing case and Ne puffing case, respectively. Confinement properties of the D_2 puffing case are described in Ref. [10].

4. Discussion

The line-averaged radiated power per unit volume, $P_{radl}(r/a)$, is measured using a set of three germanium thermistor-type bolometer arrays on a poloidal cross section at $r/a = 0$, 0.31 and 0.8 [12]. Fig. 6(a) indicates that radiative neon ions at $t = \sim 31$ ms, where the radiation power reaches a maximum, are mainly distributed around the plasma peripheral region in the case of $I_p = 350$ kA. The total plasma radiated power, P_{rad}, is estimated assuming the toroidal and poloidal symmetries of the plasma radiation and geometrical factor. P_{rad} increases up to ~ 6 MW at $t = \sim 31$ ms with Ne puffing. Radiation fraction, P_{rad}/P_{oh}, significantly increases from $\sim 15\%$ (no-gas puffing case) [12] to $\sim 60\%$, while the maximum P_{rad}/P_{oh} in the D_2 puffing case (averaged over shots) is $\sim 35\%$ [10]. Total input energy, $E_{tot}(=\int V_{loop} I_p \, dt$; $t = 0$–80 ms), in the Ne puffing case is only $\sim 5\%$ less than that in the no-gas puffing case. Therefore, the strong radiative cooling is a possible reason behind the decrease in $T_{w\text{-}ave}$ in the Ne puffing case, as shown in Fig. 5. However, the iron neutral line emission of FeI, 390.1 nm, I_{Fe} is enhanced presumably by physical sputtering of iron by neon, as shown in Fig. 6(b), while I_{Fe} decreases in the D_2 puffing case.

Alternatively, the parallel energy flux as a convective flow, Γ_E, defined as $\sim n_{e0} T_{e0}^{3/2}$ may change with gas puffing. In the cases of no-gas puffing, Ne puffing and D_2 puffing up to 200 kPa, Γ_E does not vary significantly with P_{GP} (practically, Γ_E in the Ne puffing case slightly decreases compared with that in the no-gas puffing case on average). However, in the D_2 puffing cases of 300 and 400 kPa, Γ_E decreases to less than one-half of the no-puff level as P_{GP} increases, while n_{e0} increases and T_{e0} decreases [13].

5. Summary

In order to reduce the thermal wall load due to the locked mode, fast gas puffing experiments using Ne and D_2 have been conducted in the TPE-RX RFP.

In the case of gas puffing, I_p decays and V_{loop} increases due to the increase in plasma resistance, while n_e increases and n_e profile broadens considerably. T_{e0} decreases in the Ne and D_2 puffing cases. In the no-gas puffing case, it is observed that T_w increases as I_p increases and $T_{w\text{-}max}$ reaches the melting temperature of the wall on the plasma-facing side. However, in the Ne puffing case, $T_{w\text{-}max}$ and $T_{w\text{-}avg}$ decrease. In the D_2 puffing case, $T_{w\text{-}max}$ decreases at $P_{GP} > 200$ kPa, and $T_{w\text{-}max}$ becomes half at the highest P_{GP} of 200 Pa m^3/s. This indicates that neutral gas puffing in RFP can reduce the thermal wall load.

P_{rad}/P_{oh} significantly increases from $\sim 15\%$ (no-gas puffing case) to $\sim 60\%$ (Ne puffing case), while the maximum P_{rad}/P_{oh} in the D_2 puffing case is $\sim 35\%$ on average. Therefore, radiative cooling around the plasma

peripheral region is a possible reason behind the decrease in the rate of energy flow to the wall in the Ne puffing case. Alternatively, in the D_2 puffing cases of 300 and 400 kPa, Γ_E decreases to less than one-half of the no-puff level as P_{GP} increases. The decrease in $T_{w\text{-}max}$ with P_{GP} of D_2 might be qualitatively explained by the decrease in Γ_E along the local magnetic field lines intersecting the first wall.

References

[1] M. Valisa, T. Bolzonella, L. Carraro, E. Casarotto, S. Costa, L. Garzotti, P. Innocente, S. Martini, R. Pasqualotto, M.E. Puiatti, R. Pugno, P. Scarin, J. Nucl. Mater. 241–243 (1997) 988.
[2] Y. Yagi, H. Koguchi, H. Sakakita, S. Sekine, Y. Maejima, J.B. Nilsson, T. Bolzonella, P. Zanca, Phys. Plasmas 6 (1999) 3824.
[3] Y. Yagi, S. Sekine, T. Shimada, A. Masiello, K. Hayase, Y. Hirano, I. Hirota, S. Kiyama, H. Koguchi, Y. Maejima, H. Sakakita, Y. Sato, K. Sugisaki, M. Hasegawa, M. Yamane, F. Sato, I. Oyabu, K. Kuno, T. Minato, A. Kiryu, S. Takagi, K. Sako, F. Kudough, K. Urata, H. Kaguchi, J. Orita, H. Sago, Y. Ishigami, Fusion Eng. Des. 45 (1999) 421.
[4] Y. Hirano, H. Koguchi, H. Sakakita, T. Shimada, Y. Yagi, Jpn. J. Appl. Phys. 42 (2003) 5274.
[5] L. Schmitz, R. Lehmer, G. Chevalier, G. Tynan, P. Chia, R. Doerner, R.W. Conn, J. Nucl. Mater. 176&177 (1990) 522.
[6] G.M. Staebler, G.L. Jackson, W.P. West, S.L. Allen, R.J. Groebner, M.J. Schaffer, D.G. Whyte, Phys. Rev. Lett. 82 (1999) 1692.
[7] L. Carraro, S. Costa, M.E. Puiatti, F. Sattin, P. Scarin, G. Telesca, M.Z. Tokar, M. Valisa, P. Franz, L. Marrelli, Nucl. Fusion 40 (2000) 1983.
[8] Y. Yagi, Nucl. Fusion 40 (2000) 1933.
[9] Y. Yagi, H. Sakakita, H. Koguchi, S. Sekine, Fusion Eng. Des. 46 (1999) 65.
[10] H. Sakakita, Y. Yagi, H. Koguchi, Y. Hirano, T. Shimada, A.M. Canton, P. Innocente, Jpn. J. Appl. Phys. 43, submitted for publication.
[11] Y. Yagi, S. Sekine, H. Koguchi, T. Bolzonella, H. Sakakita, J. Nucl. Mater. 290–293 (2001) 1144.
[12] H. Koguchi, Y. Yagi, Y. Hirano, T. Shimada, S. Sekine, H. Sakakita, Jpn. J. Appl. Phys. 43 (2004) 1159.
[13] Y. Yagi, H. Koguchi, H. Sakakita, Y. Hirano, Jpn. J. Appl. Phys., submitted for publication.